# Wi-PSG: Detecting Rhythmic Movement Disorder Using COTS WiFi

Wei Liu, Shan Chang, *Member, IEEE*, Ye Liu, and Hao Zhang

***Abstract*—Rhythmic movement disorder (RMD) is closely related to health problems like insomnia, daytime fatigue, anxiety disorder, and depression, or even causes severe injuries resulting from the movements. To obtain detailed information of RMD related abnormal movements for early diagnosis, there are generally three categories of solutions: 1) using camera to record image data; 2) wearing various smart devices; and 3) deploying dedicated hardware to capture sensor data. But none of such are widely accepted for different reasons due to privacy, inconvenience and excessive overhead. We believe one of the essential features in a feasible solution is *nonintrusiveness*, in which movement data collection should be carried out without the awareness of targets. In addition, it should be fairly accurate and low cost. In this work, we propose Wi-PSG, a contactless and nonintrusive sleep monitoring system, which exploits channel state information (CSI) from existing WiFi infrastructures to detect RMD related movements. Specifically, we introduce new set of sensitivity metrics and reconstruct the collected CSI into an ideal subcarrier sensitive to all target movements. With the estimated CSI background model derived from static propagation paths, nonmovement interference can be canceled from RMD movement detection.We then train the classifier for distinguishing different kinds of RMD movements using both time and frequency features extracted from CSI signals. We implement Wi-PSG with a pair of WiFi devices and wireless access point. We evaluate Wi-PSG with nine volunteers over a one-month period. The extensive experiments demonstrate that Wi-PSG can achieve a recognition accuracy of above 92%, even under challenging scenarios.**

***Index Terms*—Channel state information (CSI), commercial off-the-shelf (COTS) WiFi, movement detection, movement recognition, rhythmic movement disorder (RMD).**

## I. Introduction

RHYTHMIC movement disorder (RMD) refers to a parasomnia characterized by repetitive, involuntary rhythmic movements (typically at a frequency of 0.5–2 Hz), which may involve head, neck, trunk, or limbs either independently or in combination, occurring in association with sleep. International classification of sleep disorders version 3 (ICSD3) [1] defines three typical subtypes of those movements, i.e., *body rolling*, *head banging*, and *head rolling*. Particularly, head banging refers to vigorous anteroposterior movements of head, which usually occurs in a prone position, and head rolling tends to occur in a supine position, and is characterized by regular lateral rotation or rolling of head and neck [RMD in Children], while body rolling indicates that a sleeper rolls the entire body vigorously in an anteroposterior direction (see Fig. 1).

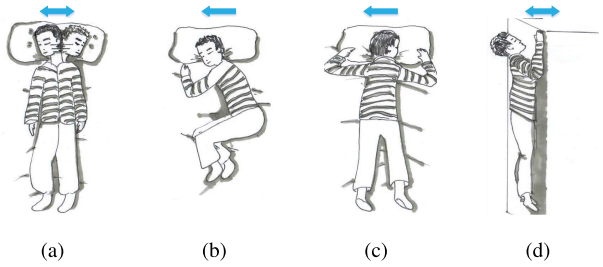


Fig. 1. RMD related movements. (a) Head rolling. (b) Body rolling (turning from supine to side). (c) Body rolling (turning from side to prone). (d) Head banging.

RMD usually occurs in infants and young children, but can also be found in adults, and may cause insomnia or excessive daytime sleepiness due to disturbed sleep, severe injuries (such as forehead bruises or other abrasions) resulting from the movements [2], as well as other negative health outcomes. For example, RMD has been correlated with attention-deficit hyperactivity disorder (ADHD) [3], and developmental disabilities, such as mental retardation or autistic spectrum disorders [4]. Most older children with persistent disorder are usually suffering from organic brain dysfunction. For a developmentally disabled adult, repeated head banging produces occipital gray matter loss and enlargement of the diploic spaces [5]. Thus, continuous historical record of abnormal movements or behaviors during sleep from an observer (or monitor) is required, such that the frequency and severity of them can be noted to assess whether the patient's movements or behaviors are at risk of injuring himself or others.

Polysomnography (PSG) is a test conducted to study sleep and to diagnose a variety of sleep disorders. It can provide specific information about unusual movements or behaviors during sleep and thus diagnose RMD. PSG requires a dozen of wired sensors attached to a patient. A critical drawback of these contact-based systems is that they may result in complications, including rashes, burns and insomnia, or even death from strangulation of infants. Moreover, PSG is typically performed in hospitals or dedicated sleep clinics rather than

Manuscript received July 14, 2020; revised September 11, 2020; accepted September 22, 2020. Date of publication October 7, 2020; date of current version March 5, 2021. This work was supported in part by the National Natural Science Foundation of China under Grant 61672151, Grant 61972081, and Grant 61772340; and in part by the DHU Distinguished Young Professor Program, Fundamental Research Funds for the Central Universities under Grant 2232020A-12. *(Corresponding author: Shan Chang.)*

The authors are with the School of Computer Science and Technology, Donghua University, Shanghai 201620, China (e-mail: liuwei628@mail.dhu.edu.cn; changshan@dhu.edu.cn).

Digital Object Identifier 10.1109/JIOT.2020.3029266

at home, and should be performed and monitored by technicians, technologists, nurses or therapists who are specifically licensed [6], which makes PSG test expensive and inconvenient. Thus, a contactless and household monitoring system holds appeal as a safer, less intrusive and more convenient alternative. Some researchers leverage the built-in inertial sensors, e.g., accelerometer, of wearable smart devices, e.g., smartwatch, to monitor a user's movements and activities during sleep [7]–[9], which, however, requires the user to wear the devices during sleep and can hardly sense small far-end body movements. Vision-based solutions are noncontact [10]–[12], however, can be significantly affected by environmental light conditions and bring privacy concerns. Similarly, audio-based schemes can be significantly degraded by the ambient noise and also give rise to privacy risks [13]–[15]. Recently, dedicated hardware/sensors (e.g., RFID readers/tags, universal software radio peripheral (USRP), frequency modulated continuous wave (FMCW) radar) and customized platforms are deployed to sense sleep related activities [16]–[18], which, however, incur high cost and low development efficiency.

To overcoming the above limitations, in this article, we present a contactless and nonintrusive sleep monitoring system, named Wi-PSG. Wi-PSG exploits channel state information (CSI) which represents amplitude and phase information for multiple orthogonal frequency division multiplexing (OFDM) subcarriers, provided by commercial off-the-shelf (COTS) WiFi, to capture and recognize RMD related abnormal movements and behaviors accurately without jeopardizing users privacy. Wi-PSG reuses existing WiFi infrastructure, and thus has no additional hardware overhead and provides rapid deployment.

Recently, two WiFi-based systems related to our work have been proposed, where CSI signals are measured for breathing monitoring during sleep [19]–[21]. Wi-Sleep [19] requires multiple transmitter (TX) and receiver (RX) pairs in order to distinguish different sleep postures. Liu *et al.* [20], [21] focused on estimating the rates of breathing and heart beating, which are at different frequencies. The authors utilize directional antennas, and separate and identify breathing and heart beating by applying band-pass filtering on the selected subcarrier which is most sensitive to those activities. However, different kinds of RMD movements are mostly at the similar frequency, and the scattering and reflecting effects caused by different movements result in different amplitude changes at each subcarrier, due to the frequency diversity of these subcarriers. It is hardly to find an optimal subcarrier which is sensitive to all kinds of movements. As a result, existing solution cannot be applied directly to RMD monitoring.

Wi-PSG uses only a single pair of WiFi device and wireless access point (AP) to continuously collect the wireless CSI of the radio signals and from which distinct patterns associated with body rolling, head banging, and head rolling can be extracted and recognized, respectively. The reuse of existing WiFi network largely increases the opportunity that Wi-PSG is widely deployed and used in home. However, achieving nonintrusive RMD monitoring using white CSI is challenging for multiple reasons.

1) Raw CSI signals contain many outliers and heavy noise, it is challenging to obtain fine-grained CSI signals reflecting minute movements and providing accurate estimation of rhythmic movements.
2) Different subcarriers have different frequencies, thus are sensitive to different kinds of movements, and represent diverse amplitude changes. It is challenging to find a subcarrier sensitive to all activities and to identify all movements accurately from the subcarrier.
3) Same kind of RMD movements may show different rhythms and amplitudes, which implies different patterns of CSI signal changes. It is challenging to extract unique features from CSI signals to identify same movements and to distinguish different kinds of movements correctly.

To solve above challenges, raw CSI signals are passed through a pipeline of filters consisted of Hampel, wavelet and moving average filters, to eliminate casual outliers and high-frequency noise, and to preserve rising/falling edges which is critical for detecting rollovers. We define a new metric to measure the sensitivity of subcarriers, which is robust to changes of environments. According to that, an ideal subcarrier representing highest sensitivity to all target movements is formed by cropping and pasting segments from different subcarriers with necessary post-processing. Then, a background model subtraction algorithm is proposed to cancel the nonmovement interference in the ideal subcarrier signal, such that amplitude peaks reflecting all kinds of RMD movements in that can be located adaptively. Finally, we carefully select a set of features from CSI signals in both time and frequency domains which are robust to environmental changes and variations of movement rhythms and amplitudes, such that, different kinds of RMD movements can be distinguished clearly. We prototype Wi-PSG using an off-the-shelf WiFi device, and conduct extensive experiments. The results show that Wi-PSG provides accurate body rolling, head banging, and head rolling estimation (rates and times) not only under typical settings but also covering challenging scenarios, including obstacles between the WiFi device and AP, and human activity interferences.

The contributions of Wi-PSG are summarized as follows.

1) To the best of our knowledge, Wi-PSG is the first system enabling nonintrusive and contactless RMD detection by reusing existing WiFi networks. Comparing with existing works [17], [22]–[25] in sleep related activities monitoring, Wi-PSG has no additional hardware overhead and provides rapid deployment.
2) We design algorithms to extract fine-grained CSI from off-the-shelf WiFi device to detect RMD movements. We also present algorithms to distinguish typical subtypes of those movements, and for all kind of movements, to provide accurate estimation of rhythms separately.
3) We implement Wi-PSG and conduct extensive experiments with nine volunteers (six adults and three children) over one month period. Experimental results show that the average detection and recognition accuracies of Wi-PSG are higher than 98% and 97%, respectively, which are comparable or even better as compared to existing dedicated sensor-based or RF-based approaches.

## II. Related Work

In general, the existing human activity sensing or recognition systems can be widely categorized as contact-based, vision/acoustics-based and RF-based approaches. In this part, we review these works and compare them with our Wi-PSG.

### A. Contact-Based Approaches

It is well known that PSG can record detailed information of human activity and ensure high sensing accuracy [6], [26], [27]. However, it usually requires user to wear a dozen of sensors which are highly expensive, invasive and uncomfortable with long-term continuous monitoring. There is a new trend that utilizes various motion sensors (e.g., magnetic, gyroscope, and accelerometer) embedded in body-attached mobile/wearable devices (e.g., smartphone [23], [24], [28] smartwatch [7]–[9], [22], and customized embedded device [29], [30]) to sense or recognize human activity. However, they also require user to wear smart devices all the time, and some people may not like to wear any device during sleeping, especially for children and elderly. In addition, these solutions cannot sense or recognize sleep related subtle head movement (e.g., head rolling).

### B. Vision/Acoustics-Based Approaches

To overcome the above-mentioned problem, a couple of studies attempt to sense or recognize human activity with contactless solutions. With the help of built-in microphone of the smartphone/smartwatch, the sound data of human activity can be recorded for further analyzing sensing performance [13]–[15], [28]. However, the performance of audio-based approaches can be significantly degraded by ambient noise. In addition, audio-based techniques also bring privacy concerns. Besides, some works used camera to monitor human activity by analyzing video stream data [10]–[12], [31], [32]. However, the vision-based approaches can be significantly affected by the environmental light conditions and also exist privacy issues.

### C. RF-Based Approaches

Recently, RF-based human activity sensing has attracted wide interest of many researchers, which relies on various wireless communication technologies, such as Radar, FMCW, USRP, RFID readers/tags, and WiFi. Specifically, Radar-based approaches are able to achieve high accuracy for monitoring sleep related activities [33]–[35]. However, they require special hardware with high frequency and incur high cost. FMCW-based approaches usually employ FMCW radar to sense human activities, such as breathing, heart rate, and gestures [18], [36]–[38]. However, they require customized hardware with a large bandwidth from 5.46 to 7.25 GHz, which is expensive and impractical. USRP-based approaches also need to deploy dedicated hardware and write complex hardware program [16], [39]–[41]. Some researchers use RFID readers/tags deployed in particular area to detect sleep related activities [17], [25], [42]. However, they often need to deploy a large number of readers/tags or dedicated devices, which limit their applications in practice. Recent studies have shown the potential of using ubiquitous WiFi devices to monitor human activity [19], [20], [43]–[48]. They utilize CSI extracted from WiFi signals to capture the environmental changes caused by human body movement. However, these approaches either need to deploy dedicated high gain directional antennas at the TX/RX to improve the power of reflected signals or cannot both detect and recognize sleep related activities simultaneously, especially for subtle head movement. More importantly, it is hardly to find an ideal subcarrier which is sensitive to all kinds of movements by using existing works. Without obtaining the ideal subcarrier, detecting and recognizing RMD movements with high accuracy are challenging.

Different from the existing works, we propose Wi-PSG, which is a device-free system in indoor environment, to detect RMD movements by utilizing existing ubiquitous COTS WiFi directly. The proposed system achieves real-time movement detection, and recognizes different RMD movements (i.e., head rolling, supine to side, side to prone, and head banging) without wearing any sensors or deploying any dedicated devices. Specifically, we extract CSI amplitude measurements from WiFi signals transmitted by COTS WiFi to capture motion state information caused by RMD movements. A novel subcarrier reconstruction algorithm and a novel background model-based peak detection algorithm are proposed to improve the performance of movement detection. Moreover, we combine time-domain features with frequency-domain features of CSI amplitudes together to enhance the performance of movement recognition. Comparing with the existing works [9], [19], [47], Wi-PSG significantly boost the movement detection accuracy of sleep related activities (i.e., supine to side, side to prone and head banging) to 100%.

## III. Preliminaries

WiFi devices with IEEE 802.11n/ac standards use multiple input multiple output (MIMO) system. A WiFi channel with MIMO is divided into multiple orthogonal subcarriers by OFDM. CSI, as the physical radio frequency of channel property of subcarriers transformed by OFDM, represents how wireless signals propagate from the TX to the RX at certain subcarrier frequencies along multiple paths, and can be extracted and analyzed through commercial WiFi devices. The amplitude and phase of CSI are impacted by the displacements and movements of the TX, RX, surrounding objects and humans. It implies the wireless characteristics of nearby environments can be captured by a time series of CSI measurements, which is the rationale for CSI being used for WiFi sensing.

When a WiFi signal transmitted by a TX to its intended RX, if there is no obstacle between them, then the signal will propagate directly in a straight line from the TX to the RX. Such a straight path is named as line-of-sight (LOS) path. Besides this, the RX might also receive signals which are reflected by either static or dynamic surrounding objects and humans. In other words, the signals travel through nonline-of-sight (NLOS) paths. For example, in Fig. 2(a), when a person is supine between a pair of TX and RX and rolling its head,

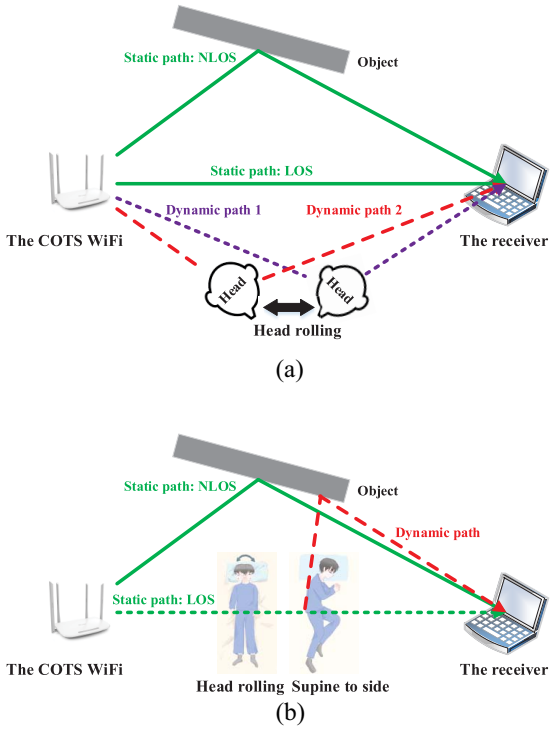


Fig. 2. Rationale of using CSI for detecting different RMD movements. (a) Head rolling. No change on the static propagation paths. (b) Body rolling (turning from supine to side). The static LOS propagation path is converted to dynamic path.

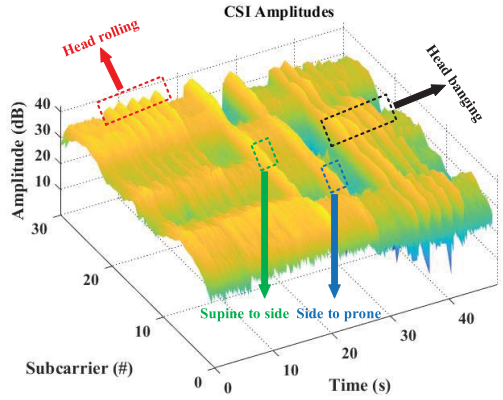


Fig. 3. CSI amplitudes obtained during the experiment.

there exist LOS path, and two kinds of NLOS paths, i.e., static reflected path caused by the wall, and dynamic reflected path caused by head rolling. While in Fig. 2(b), if the person is rolling its whole body, the LOS path might be covered by its body repetitively, as long as the person is lying on its side. In both situations, body and head movements will cause the change of dynamic NLOS paths (i.e., purple and red dotted lines in Fig. 2), which implies the change of CSI signals received by the RX. Actually, with the rhythmic movements of body/head, the CSI amplitudes will show the ripple-like pattern which can be seen in Fig. 3. It should be also noticed that, in the second situation, not only NLOS paths, but also the LOS path changes over time as well, which implies that the

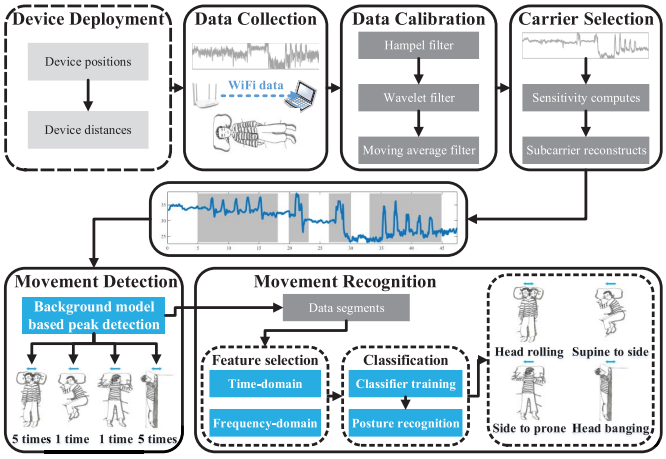


Fig. 4. System architecture of Wi-PSG.

static propagation paths change continuously, and it is difficult to estimate CSI signals propagating along static paths for the purpose of extracting CSI signals propagating along dynamic paths from the mixed CSI signals received by the RX.

## IV. System Design

In this section, we introduce the system design of Wi-PSG, including system overview, data collection, data calibration, subcarrier selection, movement detection, and movement recognition.

### A. System Overview

The basic idea of Wi-PSG is to detect and recognize abnormal movements during sleep through capturing the unique patterns embedded in WiFi signals. Wi-PSG takes time series of CSI amplitude measurements as input. Considering that CSI amplitude measurements are affected by the deployment of the TX–RX pair, Wi-PSG requires an initialization procedure to decide an effective layout of the TX–RX pair (discussed in Section V-B) before use. Then, Wi-PSG operates in a sequential manner as shown in Fig. 4.

1) *CSI Data Collection:* Time series of CSI amplitude measurements are collected at an off-the-shelf WiFi device by utilizing existing WiFi traffic or system-generated periodic traffic (if network traffic is insufficient) generated by a wireless AP.
2) *CSI Data Calibration:* The raw CSI amplitude measurements contain outliers, and heavy noise imposed by the environment and hardware devices (see Fig. 5), Wi-PSG removes them by a pipeline of filters consisted of Hampel, wavelet and moving average filters.
3) *Subcarrier Selection:* The CSI amplitudes of a subcarrier have different sensitivity to different RMD movements due to diversity of signal propagation path. Wi-PSG quantifies the sensitivity of each subcarrier in a variable-size moving time window. Based on that, an ideal subcarrier having highest sensitivity to all target movements is constructed.
4) *Movement Detection:* This module identifies all amplitude peaks on the CSI time series of the ideal subcarrier,

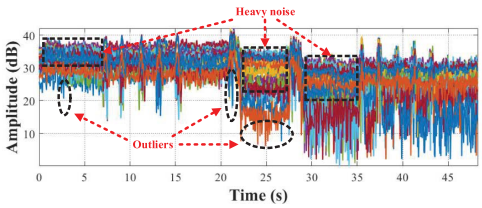


Fig. 5. CSI subcarriers before data calibration.

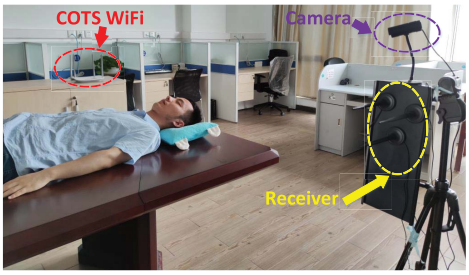


Fig. 6. Experiment setup using the COTS WiFi.

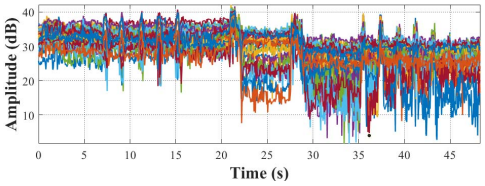


Fig. 7. CSI subcarriers after applying Hampel filter.

TABLE I
TEST SCENARIO FOR DETECTING RMD MOVEMENTS

| Stage# | Time duration | RMD related movements |
|---|---|---|
| Stage1 | 0s $\sim$ 5s | Supine (non-movement) |
| Stage2 | 6s $\sim$ 17s | Head rolling (2s/time, 5 times) |
| Stage3 | 18s $\sim$ 25s | Body rolling (supine to side, 1 time) |
| Stage4 | 26s $\sim$ 34s | Body rolling (side to prone, 1 time) |
| Stage5 | 35s $\sim$ 46s | Head banging (2s/time, 5 times) |

each of which implies an RMD movement, using a peak detection algorithm base on background model.

5) *Movement Recognition:* Wi-PSG extracts a series of effective features that uniquely correlated to RMD movements. The extracted features are used to train a multiclass SVM classifier such that typical RMD movements, including body rolling (divided into two stages, i.e., turning from supine to side, and from side to prone), head rolling and head banging can be distinguished.

### B. Empirical CSI Collection

To study the characteristics of CSI signals related to RMD related movements and behaviors, we conduct a data collection campaign in our laboratory (as illustrated in Fig. 6) with an 802.11n WiFi network, where a single off-the-shelf WiFi device (i.e., Lenovo laptop equipped with Intel 5300 NIC as the RX) connected to a commercial wireless AP (i.e., TP-Link WDR5620 as the TX). The relative distance between the TX and RX is 2.5 m. A volunteer lying between the TX–RX pair is asked to take actions and change his postures according to Table I. In this experiment, we divide a body rolling into two procedures, i.e., the volunteer changes its sleeping position from supine to side, and then from side to prone (or in opposite directions). We use developed CSI-Tools [49] to obtain 30 out of 56 time-series CSI measurements of OFDM subcarriers [19] as input of Wi-PSG, which are collected at the RX by utilizing periodic packet transmissions (system-generated) from the TX to RX during the experiments. The packet transmission rate is set to 20 pkts/s. The operating frequency band is set to 2.4 GHz.

### C. CSI Data Calibration

Original CSI measurements contain heavy noise which could come from environment-related changes, radio signal interference, etc. To improve the reliability of the CSI measurements, it's necessary to mitigate the noise presented in the collected CSI samples. We consider three kinds of noise, i.e., *outliers* which have significant different values from other neighboring CSI measurements, *high-frequency noise* which is unlikely to be caused by RMD related movements as they usually present in a fixed and lower frequency range, *low-frequency white noise* which presents in the same frequency range as RMD related movements, and apply a series of filters to remove those noise consecutively.

*1) Removing Outliers With Hampel Filter:* Fig. 5 illustrates the original time series of CSI amplitude from all subcarriers collected in the data collection campaign described before. It can be seen that outliers, exhibiting abrupt changes, are ubiquitous in subcarriers (e.g., around 3, 22, and 25 s). We employ Hampel filter with a sliding window at each subcarrier to remove outliers. In specific, given a CSI time series on $i$th subcarrier with $n$ measurements, denoted as $C^i = \{c_1^i, \ldots, c_n^i\}$, and $k$th sliding window of size $\Phi$, i.e., $W_k^i = \{c_k^i, \ldots, c_{k+\Phi-1}^i\}$ $(1 \leq k \leq n - \Phi + 1)$, Hampel filter regards any $c_j^i$ $(k \leq j \leq k + \Phi - 1)$ in the sliding window $W_k^i$ falling out of the closed interval $[\mu_k^i - \gamma \times \sigma_k^i, \mu_k^i + \gamma \times \sigma_k^i]$ as an outlier, where $\mu_k^i$ and $\sigma_k^i$ are the median and the standard deviation (SD) of $W_k^i$, respectively, and $\gamma$ is a constant scale factor [19]. The outlier $c_j^i$ will be replaced by $\mu_k^i$. We empirically set $\gamma$ and $\Phi$ as 1.5 and 7, respectively. Fig. 7 demonstrates the time series of CSI amplitude after applying Hampel filter. It can be seen that all the identified outliers have been removed.

*2) Removing High-Frequency Noise With Wavelet Filter:* Conventional low-pass filters like Butterworth and Chebyshev not only suppress high-frequency noise but also flatten rising/falling edges appeared in time series of CSI amplitude, which is however critical for detecting RMD related movements. For example, Fig. 8 depicts time series of CSI amplitude from no. 1, 18, and 30 subcarriers. It can be seen

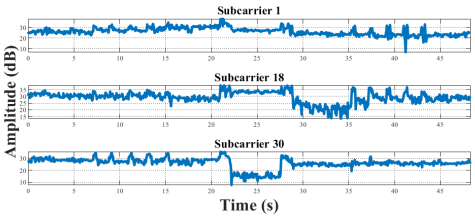


Fig. 8. CSI amplitudes of three subcarrier over time after applying Hampel filter.

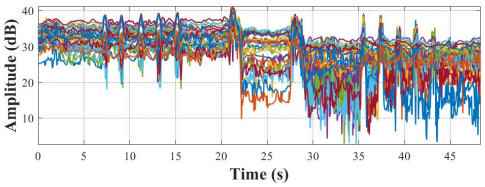


Fig. 9. CSI subcarriers after applying wavelet filter.

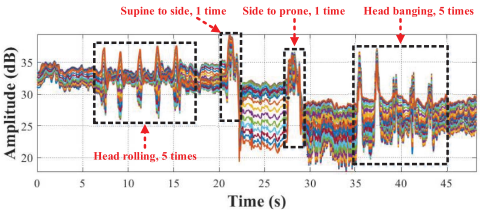


Fig. 10. CSI subcarriers after applying moving average filter.

that CSI amplitude measurements of no. 30 subcarrier display a sudden drop and surge when the volunteer changes its sleeping position from supine to side (i.e., around 22 s), and from side to prone (i.e., around 28 s), respectively. Thus, it is required to eliminate high-frequency noise while preserving those rising/falling edges in CSI time series. We apply the wavelet filter proposed in [50] since it can preserve extremely well the sharp transitions in signals than the other low-pass filters [19]. In specific, we use the principle of Stein's unbiased risk as threshold selection rule, and soft thresholding as filter. Finally, we adopt four-level "db4" wavelet transform on each CSI subcarrier and use only the approximation coefficients to filter high-frequency noise to extract low-frequency useful signals. Fig. 9 shows the time series of CSI amplitude of all subcarriers after applying wavelet filter. It can be seen that high-frequency oscillations are suppressed and rising/falling edges are preserved properly. Fig. 9 shows the time series of CSI amplitude of all subcarriers after applying wavelet filter. It can be seen that high-frequency oscillations are suppressed and rising/falling edges are preserved properly.

*3) Removing White Noise With Moving Average Filter:* Wavelet filter cannot deal with those white noises whose frequency band overlap with signals. Thus, we use a moving average filter with a Gaussian window to restrain white noise contained in CSI signals further. The size of the Gaussian window is empirically set as 20. Fig. 10 displays the resulted time series of CSI amplitude of all subcarriers after applying moving average filter to the outputted CSI signals of the wavelet filter. It can be seen that all CSI signals are more smooth and neat, and all RMD related movements can be roughly identified by their amplitude variations.

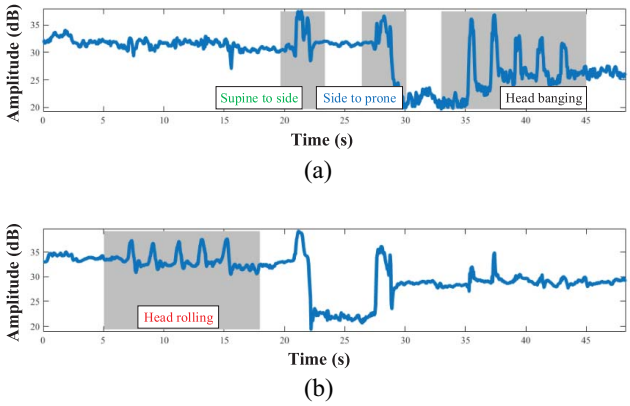


Fig. 11. Results of RMD detection at different subcarriers. (a) Subcarrier 18 after data calibration. (b) Subcarrier 30 after data calibration.

### D. Subcarrier Selection

After CSI data calibration, it is desired to find a subcarrier whose time series of CSI amplitude shows clear correlation (i.e., sensitive) with all RMD related movements. However, due to frequency (and wavelength) diversity, for a given movement, the amplitudes of different subcarriers represent different sensitivity. Thus, a subcarrier sensitive to all RMD related movements may not exist. Fig. 11(a) and (b) depict the time series of CSI amplitude on no. 18 and no. 30 subcarriers, respectively. It can be seen that the CSI amplitude on no. 18 subcarrier demonstrates high sensitivity to body rolling and head banging, and is, however, insensitive to head rolling, while the CSI amplitude on no. 30 subcarrier is closely related to head and body rolling, but not affected by head banging. Therefore, it may not be possible to find such a subcarrier exhibiting tight correlation with all RMD related movements. To solve this problem, we intend to construct an ideal subcarrier representing highest sensitivity to all target movements by cropping and pasting segments from different subcarriers. In the example of Fig. 11, we can extract a sequence of CSI amplitude (in gray area) on no. 30 subcarrier to replace the corresponding sequence (i.e., with the same time interval) of CSI amplitude on no. 18 subcarrier, and obtain a new synthetic subcarrier, which can capture all RMD related movements.

Furthermore, we propose a new definition of sensitivity of subcarriers as follows.

*Definition 1 (Sensitivity):* Given a time series of CSI amplitude on $i$th subcarrier, i.e., $C^i = \{c_1^i, \ldots, c_n^i\}$, the sensitivity of $C^i$ can be calculated by

$$Q_{(1,n)}^i = (1-\theta) \times sd^i + \theta \times kt^i \tag{1}$$

$$kt^i = \frac{\frac{1}{n}\sum_{j=1}^{n}\left(c_j^i - \bar{c}\right)^4}{\left(\frac{1}{n}\sum_{j=1}^{n}\left(c_j^i - \bar{c}\right)^2\right)^2} - 3 \tag{2}$$

where $sd^i$ and $kt^i$ are the SD and kurtosis of $C^i$, respectively. $\theta$ is a weighting factor and its range is [0, 1]. Note that our new definition about subcarrier's sensitivity is different from the

**Algorithm 1** Sensitivity-Based Carrier Reconstruction

**Input:** given time series of CSI amplitude on the 30 subcarriers: each of which is denoted as $C^k_{(1,n)} = \{c^k_1, \dots c^k_n\}$ ($1 \le k \le 30$); original window size: $l$; weighting factor: $\theta$; reduced size of the time window: $\delta$;

**Output:** the reconstructed ideal subcarrier: $\tilde{C}$;

1: $\tilde{C} \leftarrow \emptyset$; %Initialize ideal subcarrier
2: $w_s \leftarrow 1, w_e \leftarrow l$; %Initialize the staring and ending points of the time window
3: **while** $(length(\tilde{C}) < n)$ **do**
4: $\quad Q \leftarrow 0$;
5: $\quad Q^{max} \leftarrow 0$;
6: $\quad w_s^{max} \leftarrow 0, w_e^{max} \leftarrow 0, k^{max} \leftarrow 0$;
7: $\quad$ **for** $k = 1{:}30$ **do**
8: $\quad\quad w_e \leftarrow min(w_s + l - 1, n)$;
9: $\quad\quad$ **while** $(w_s < w_e)$ **do**
10: $\quad\quad\quad s_w \leftarrow w_e - w_s$; %Size of the time window
11: $\quad\quad\quad \bar{c}^k \leftarrow \frac{1}{s_w}\sum_{j=1}^{s_w} c^k_j$; %Segmentation threshold
12: $\quad\quad\quad$ **if** $c^k_{w_e} \le \bar{c}^k$ **then**
13: $\quad\quad\quad\quad sd^k = \sqrt{\frac{1}{s_w}\sum_{j=1}^{s_w}(c^k_j - \bar{c}^k)}$;
14: $\quad\quad\quad\quad kt^k = \frac{\frac{1}{s_w}\sum_{j=1}^{s_w}(c^k_j - \bar{c}^k)^4}{(\frac{1}{s_w}\sum_{j=1}^{s_w}(c^k_j - \bar{c}^k)^2)^2} - 3$;
15: $\quad\quad\quad\quad Q \leftarrow (1-\theta) \times sd^k + \theta \times kt^k$; % Sensitivity
16: $\quad\quad\quad\quad$ **break**;
17: $\quad\quad\quad$ **else**
18: $\quad\quad\quad\quad w_e \leftarrow w_e - \delta$; % Reducing the window size
19: $\quad\quad\quad$ **end if**
20: $\quad\quad$ **end while**
21: $\quad\quad$ **if** $Q > Q^{max}$ **then**
22: $\quad\quad\quad Q^{max} \leftarrow Q$;
23: $\quad\quad\quad w_s^{max} \leftarrow w_s, w_e^{max} \leftarrow w_e, k^{max} \leftarrow k$;
24: $\quad\quad$ **end if**
25: $\quad$ **end for**
26: $\quad \tilde{C} \leftarrow \tilde{C} + C^{k^{max}}_{(w_s^{max}, w_e^{max})}$;
27: $\quad w_s \leftarrow w_e^{max} + 1$;
28: **end while**

existing scheme which only utilizes the variance of CSI amplitude to quantify the subcarrier's sensitivity [20]. We introduce a new metric called *kurtosis* to enhance its robustness. The reason we introduce it is that higher kurtosis value usually represents a sharper CSI amplitude peak so that the real peaks reflecting RMD movements can be captured more accurately using our new definition.

Then, we use a sensitivity-based method (Algorithm 1) to construct a time series of CSI amplitude from an ideal subcarrier for RMD movements detection. Specifically, Given time series of CSI amplitudes on the 30 subcarriers, each of which is denoted as $C^k_{(1,n)} = \{c^k_1, \dots, c^k_n\}$ ($1 \le k \le 30$), to form a new time series of CSI amplitude $\tilde{C}_{(1,n)}$, a simple way is to cut each $C^k_{(1,n)}$ into several equal size segments (except the last segment) using a series of consecutive time windows

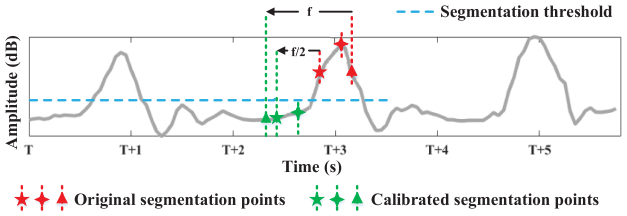


Fig. 12. Illustration of segmentation point calibration.

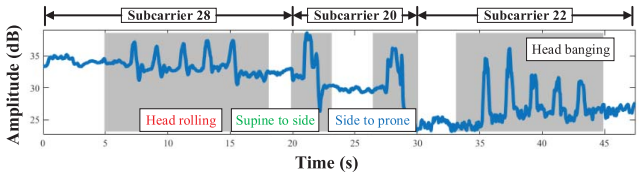


Fig. 13. Reconstructed ideal subcarrier.

of size $l$ (without overlap), and for each time window $W_{\tau_j}$, where $1 \le j \le \lceil (n/l) \rceil$, and $\tau_j$ represents the time interval $[(j-1) \times l + 1, j \times l]$, quantify the sensitivity of each $C^k_{(1,n)}$ in it, and $C^{k^{\max}}_{\tau_j}$, which has the maximum sensitivity in each window $W_{\tau_j}$, will be extracted and concatenated to form $\tilde{C}_{(1,n)}$.

However, using such a fixed size time window, it is possible that a sequence of CSI amplitudes corresponding to a movement is truncated by a window, i.e., the ending point of the sequence in the window is located close to an amplitude peak (an example is illustrated in Fig. 12), which may lead to failures of detecting and recognizing the movement. To address this problem, we use a variable-size time window of initial size $l$, and adjust the size of it if necessary. In particular, once apply a window $W^k_{(1,l)}$ to $C^k_{(1,n)}$, we check if the constraint that the amplitude of the ending point in $W^k_{(1,l)}$, i.e., $c^k_l$, is smaller than the mean in $W^k_{\tau_1}$ can be satisfied, if so, $W^k_{(1,l)}$ will be adopted, otherwise, $W^k_{(1,l)}$ will be reduced backward by $\delta$, obtaining $W^k_{(1,l-\delta)}$, and the ending point in the current window $W^k_{(1,l-\delta)}$ will be rechecked until the above constraint can be satisfied, as shown in lines 1–18 of Algorithm 1. Then the sensitivity of $C^k_{(1,n)}$ will be quantified in the current time window $W^k_{(1,l-g\times\delta)}$ ($g \times \delta < l - 1$). We select $C^{k^{\max}}_{(1,l-g\times\delta)}$ with maximum sensitivity in its own time window $W^k_{(1,l-g\times\delta)}$ as the first segments of $\tilde{C}_{(1,n)}$, and $W^k_{(1,l-g\times\delta)}$ is considered as the first global time window, and is applied to time series of CSI amplitudes on all other subcarriers as well. We perform the above procedure on the left parts of time series of CSI amplitude on all subcarriers, i.e., $C^k_{(l-g\times\delta+1,n)}$, $k = 1, \dots, 30$, iteratively, until $\tilde{C}_{(1,n)}$ constructed, as shown in lines 19–28 of Algorithm 1.

In addition, when concatenating two segments $C^{i^{\max}}_{(a,b)}$, and $C^{j^{\max}}_{(b+1,c)}$, to avoid sudden jump of amplitude between point $c^{i^{\max}}_b$ and $c^{j^{\max}}_{b+1}$, we choose a sequence of data points across the two segments, i.e., $S = \{c^{i^{\max}}_{b-f}, \dots, c^{i^{\max}}_b, c^{j^{\max}}_{b+1}, \dots, c^{j^{\max}}_{b+f}\}$, and conduct the moving average smoothing on $S$ to obtain a smooth version of it. In this way, for any movement, the

**Algorithm 2** Background Model-Based Peak Detection

**Input:** given a time series of CSI amplitude on an ideal subcarrier $\tilde{C}_{(1,M\times L)} = \{c_1, \ldots, c_{(M\times L)}\}$; packet transmission rate $r_p$; maximum possible movement frequency $f_{rm}$; maximum possible ambient interference $\epsilon$;

**Output:** real peak set: *PeakSet*

*PeakSet* $\leftarrow \emptyset$;
*MaxSet* $\leftarrow$ *FindLocalMaxs*$(\tilde{C}_{(1,M\times L)})$;%*MaxSet* $= \{m_k, 1 \leqslant k \leqslant K\}$;
$d \leftarrow \frac{r_p}{f_{rm}}$; %Set minimum peak-to-peak interval
**for** $\omega = 1 : M$ **do**
  **if** $\omega == 1$ **then**
    $B^{(\omega)} \leftarrow Mean(\tilde{C}^{(\omega)})$;
  **else**
    $\alpha^{(\omega)} \leftarrow \frac{\left|Mean(\tilde{C}^{(\omega)}) - B^{(\omega-1)}\right|}{Max(Mean(\tilde{C}^{(\omega)}), B^{(\omega-1)})}$; %Updating rate
    $B^{(\omega)} \leftarrow (1-\alpha^{(\omega)}) \times B^{(\omega-1)} + \alpha^{(\omega)} \times Mean(\tilde{C}^{(\omega)})$;
    $B^{(\omega-1)} \leftarrow B^{(\omega)}$;
  **end if**
  **for** each $m_k \in MaxSet$ in $\tilde{C}^{(\omega)}$ **do**
    **if** $amplitude(m_k) < B^{(\omega)} + \epsilon$ **then**
      delete $m_k$ from *MaxSet*;
    **end if**
**end for**
Sort *MaxSet* by amplitude in descending order, obtaining $\{m_{d_1}, ..., m_{d_v}\}$;
Add $m_{d_1}$ into *PeakSet*;
**for** $i = d_2 : d_v$ **do**
  **for** each peak $p_j$ in *MaxSet* **do**
    **if** $(location(m_i) - location(p_j)) \geqslant d$ **then**
      add $m_i$ in *PeakSet*;
    **end if**
  **end for**
**end for**
**Return** *PeakSet*.

most sensitive segment of CSI amplitude among all subcarriers is reserved. Consequently, we consider that the resulted time series of CSI amplitude is from an ideal subcarrier which is sensitive to all RMD related movements and behaviors. We empirically set $\theta$, $\delta$, and $l$ as 0.6, $(f/2)$ ($f$ is the sampling rate) and $5f$, respectively.

Fig. 13 illustrates the synthetic time series of CSI amplitude after applying Algorithm 1 to all subcarriers in Fig. 10. The ideal subcarrier is composed of three subcarriers, i.e., no. 28 (0–20 s), 20 (20–30 s), and 22 (30–47 s) subcarriers. It can be seen that the fluctuations in reconstructed time series of CSI amplitude correspond to all movements prescribed in our experiment.

### *E. Movement Detection*

From Fig. 13, we observe the CSI amplitudes on the ideal subcarrier presents some ripple-like pattern over time which corresponds to rhythmic movements. This observation suggests that we can identify RMD related movements (including the number of times and durations) by finding all peaks and calculating peak-to-peak intervals of CSI amplitude time series

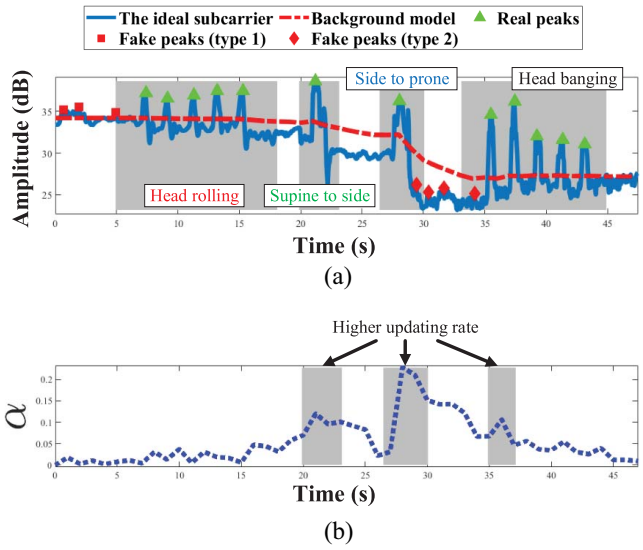


Fig. 14. Illustration of background model-based peak detection. (a) Result of peak detection. (b) Change of updating rate $\alpha$.

on the ideal subcarrier. We thus first identify peaks of CSI amplitude. The typical peak finding algorithm determines a data sample as a peak if its value is larger than its two neighboring samples [20]. However, such simple method produces many fake peaks (i.e., the identified peaks that are not at the location of real peaks of the CSI time series implying rhythmic movements) as illustrated in Fig. 14(a), e.g., fake peaks (type 2). In order to filter out fake peaks, two thresholds might be applied, i.e., the minimum vertical distance from a local peak to its neighboring valleys (relative height), and the minimum height of a peak (absolute height). Intuitively speaking, peaks that are smaller or lower than the corresponding thresholds will be removed. However, various factors could affect the relative height of peaks, for example, kinds and amplitudes of rhythmic movements, determining the minimum relative height of peaks is very hard. Meanwhile, as we mentioned before, in many cases, not only dynamic but also static propagation paths of CSI signals (i.e., the background model) change over time. As we know, if a person lays still in a certain position, e.g., supine, then both dynamic and static propagation paths of CSI signals are unchanged, which means CSI amplitudes of each subcarrier remain stable. Once the person turns from supine to prone position, the static propagation paths of CSI signals could be changed, which implies the CSI amplitude of a subcarrier could be changed to another steady value. While, if the person moves some parts of its body periodically lying in two different positions, e.g., rolling its head in supine position and banging its head in prone position, respectively, then the periodical change of dynamic CSI signal propagation paths will lead to oscillations of CSI signals on their respective baseline values of amplitudes. It means that absolute height of peaks in the two cases will be different due to different baseline values of CSI amplitudes in supine and prone positions. As a result, it is also hardly to determine a threshold of absolute height of peaks for distinguishing fake peaks from real peaks. For example, in Fig. 13, we cannot choose a threshold of the absolute height of peaks to

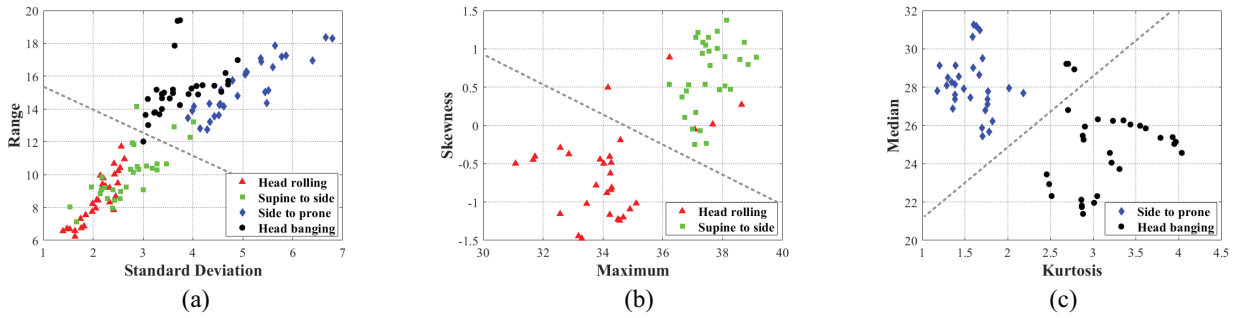


Fig. 15. Combination of different features for distinguishing different RMD movements. (a) SD and range. (b) Maximum and skewness. (c) Kurtosis and median.

TABLE II
FEATURES USED IN WI-PSG

| Time-domain | Frequency-domain |
|---|---|
| mean, median, maximum, minimum, range, variance, standard deviation, kurtosis, skewness, sensitivity | subcarrier with maximum sensitivity |

obtain all real peaks without introducing fake peaks. Note that we actually mind those fluctuations caused by the changes of dynamic propagation paths of CSI signals. We propose to estimate the amplitude of static propagation paths of CSI signals (i.e., background model reflecting nonmovement interference of multipath transmission), and subtract them from amplitudes of CSI signals. Then, only those peaks above the background model are considered as real peaks.

In detail, given a time series of CSI amplitude on an ideal subcarrier $\tilde{C}_{(1,M\times L)} = \{c_1, \ldots, c_{(M\times L)}\}$, we use a sliding window of size $L$ without overlap to conduct piecewise estimation of its background model. In other word, $\tilde{C}_{(1,M\times L)}$ will be separated into $M$ segments, and $\tilde{c}_l^{(\omega)}$ $(1 \le \omega \le M,\ 1 \le l \le L)$ represents the $l$th amplitude in $\omega$th segments of $\tilde{C}_{(1,M\times L)}$. The background model $B^{(\omega)}$ of $\tilde{C}^{(\omega)}$ can be calculated by

$$B^{(\omega)} = \begin{cases} \text{Mean}\left(\tilde{C}^{(\omega)}\right) = \frac{1}{L}\sum_{l=1}^{L} c_{L\times(\omega-1)+l} \\ \qquad\qquad\qquad\qquad \text{if } \omega = 1 \\ \left(1-\alpha^{(\omega)}\right)\times B^{(\omega-1)} + \alpha^{(\omega)} \times \text{Mean}\left(\tilde{C}^{(\omega)}\right), \quad \text{else} \end{cases} \tag{3}$$

where $\alpha^{(\omega)} \in [0, 1]$ is the updating rate [51], and is calculates by

$$\alpha^{(\omega)} = \frac{\left|\text{Mean}\left(\tilde{C}^{(\omega)}\right) - B^{(\omega-1)}\right|}{\text{Max}\left(\text{Mean}\left(\tilde{C}^{(\omega)}\right), B^{(\omega-1)}\right)}. \tag{4}$$

It can be seen that $\alpha^{(\omega)}$ changes adaptively according to the variance of $\tilde{C}^{(\omega)}$. After estimating the background model $B^{(\omega)}$, in $\tilde{C}^{(\omega)}$, only those peaks whose amplitudes are larger than $B^{(\omega)}$ plus a small value $\epsilon$ will be considered as real peaks. $\epsilon$ is the maximum possible ambient interference. In other word, $B^{(\omega)} + \epsilon$ is the threshold of absolute height of peaks, i.e.,

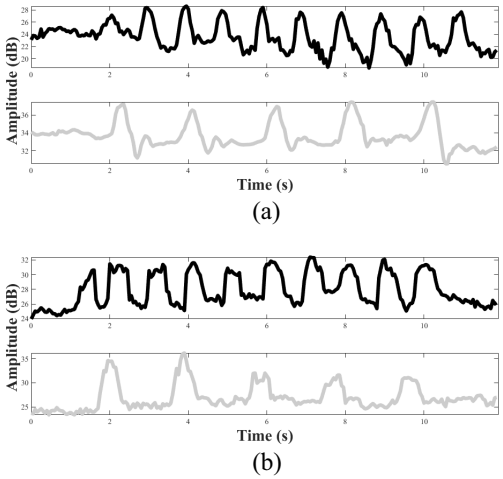


Fig. 16. Different CSI amplitude patterns. (a) Head rolling (1 Hz versus 0.5 Hz). (b) Head banging (1 Hz versus 0.5 Hz).

fake peaks (type 1) shown in Fig. 14(a) will be removed. In addition, we apply another threshold $d$ to the minimum distance between two neighboring peaks based on the human's maximum possible frequency $f_{rm}$ of rhythmic movements, and the sampling rate of CSI amplitudes that corresponds to WiFi packet transmission rate $r_p$, to further reduce the number of fake peaks, i.e., $d = (r_p/f_{rm})$. In particular, we set $f_{rm}$, $r_p$, and $\epsilon$ as 1 Hz, 20 pkts/s, and 2 dB, respectively. In our experiments, we observe that a short sliding window of three second is good enough to obtain precise estimation of background model. The background model-based peak detection algorithm is provided in Algorithm 2.

As described in lines 1 and 2 of Algorithm 2, Wi-PSG first finds all the candidate peaks with local maximum using typical peak finding algorithm. Then, Wi-PSG calculates the updating rate $\alpha$ so that the background model in the current local time window can be estimated, as shown in lines 3–11 of Algorithm 2. After that, as shown in lines 12–16 of Algorithm 2, Wi-PSG deletes the fake peaks from the candidate peaks according to the background model estimated and the maximum possible ambient interference. Finally, Wi-PSG further removes fake peaks according to the minimum distance between two neighboring peaks based on the human's maximum possible movement frequency and the sampling rate, as shown in lines 17–26 of Algorithm 2.

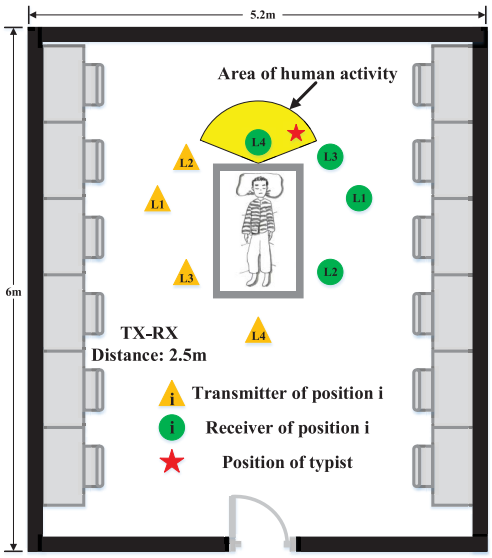


Fig. 17. Experimental setup scenario.

Fig. 14(a) illustrates the peaks founded by applying Algorithm 2 to the time series of CSI amplitude on the ideal subcarrier shown in Fig. 13. The red dotted line represents the background model estimated, which is able to adapt the change of CSI amplitudes. In other words, nonmovement interferences existed in CSI amplitude measurements can be measured automatically and accurately no matter the change of RMD movement postures. It can be seen from Fig. 14(a) that all the real peaks reflecting RMD movements are detected without any fake peaks by applying Algorithm 2.

Fig. 14(b) shows the variation of updating rate $\alpha$ with time. It can be seen that the updating rate $\alpha$ is able to adapt the change of nonmovement interferences caused by the change of RMD movement postures. Specifically, the updating rate $\alpha$ becomes higher when the users change their movement postures from one to another (i.e., around 21, 28, and 36 s). Thus, the estimated background model reflecting nonmovement interference of multipath transmission is able to adapt the change of CSI amplitudes. The results demonstrate the robustness and effectiveness of updating rate $\alpha$.

### F. Movement Recognition

*1) Feature Extraction:* Different kinds of rhythmic movements imply different health problems [4], [52]. For example, head rolling or head banging usually causes insomnia, depression and physical injury. Prone could result in obstructive sleep apnea, especially for children. Therefore, it is necessary to distinguish different kind of rhythmic movements, i.e., head rolling and banging, and body rolling (turning from supine to side, and from side to prone), which facilities the diagnosis of potential sleep disorder diseases.

To this end, for each peak $\tilde{c}_p$ in $\tilde{C}$, we find its two neighboring valleys (i.e., local minimums before and after $\tilde{c}_p$) $\tilde{c}_{vb}$ and $\tilde{c}_{va}$ ($vb \leq p \leq va$) which are below the background model. We employ $\tilde{c}_{(vb,va)} = \{\tilde{c}_{vb}, \ldots, \tilde{c}_{va}\}$ as a unit to extract features to characterize the rhythmic movement corresponding to $\tilde{c}_p$. Intuitively, different kinds of rhythmic movements may display different shapes of CSI amplitude curves. For example, it can

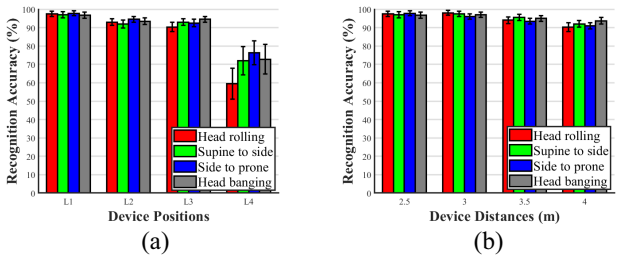


Fig. 18. Impact of device positions and distances. (a) Recognition accuracy under different device positions. (b) Recognition accuracy under different device distances.

be seen in Fig. 13, head rolling causes smaller fluctuations, and head banging implies higher kurtosis of CSI amplitudes, comparing with other RMD related movements. Thus, we extract six statistics features in time domain from the sequence of CSI amplitude $\tilde{c}_{(vb,va)}$, including SD, range (i.e., *maximum–minimum*), maximum, median, kurtosis, and skewness, which are commonly used to measure the distribution of data. We study the efficacy of these features and have the following observations. First, the combination of range and SD can separate head rolling and turning to side from head banging and turning to prone [see Fig. 15(a)]. Second, the combination of skewness and maximum can roughly distinguish head rolling from turning to side. Third, the combination of kurtosis and median is effective in distinguishing turning to prone from head banging.

Furthermore, we observe that same kind of movements may show different rhythms and amplitudes, even for the same person, implying different patterns of CSI signals (see Fig. 16), which leads to misclassifications. To solve this problem, recall that different subcarriers have different sensitivities to the same kind of rhythmic movements, we therefore introduce a novel frequency-domain feature, i.e., subcarrier with maximum sensitivity, and four extra time-domain features, i.e., mean, minimum, variance and sensitivity, to enhance the robustness of movement recognition, as listed in Table II.

*2) Training and Classification:* Given the extracted CSI features, Wi-PSG uses them as inputs to train a classifier for distinguishing four different kinds of RMD movements. Although deep neural networks (DNNs)-based classifiers are powerful for multiclass classification, they always require a huge number of training samples. It is inconvenient for people to take a very long time for training data collection. Instead, A multiclass support vector machine with the radial basis function (RBF) kernel function is trained. In particular, SVMs are inherently two-class classifiers. Thus, we use a common way to build a four-class SVM classifier in which four two-class one-against-all classifiers are trained, and the class that is selected by the most classifiers is chosen. The $m$th one-against-all SVM is trained with all of the samples in the $m$th class with positive labels, and all other samples with negative labels.

## V. Evaluation

In this section, we first introduce the implementation of Wi-PSG. Then, we investigate the deployment of the AP and WiFi

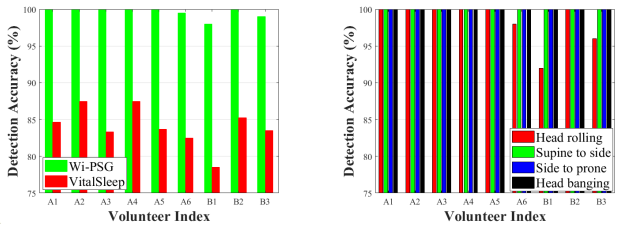


Fig. 19. Performance of movement detection. (a) Detection accuracy (Wi-PSG versus VitalSleep). (b) Detection accuracy of different RMD movements.

device to obtain an appropriate device layout to improve detection performance. Next, we evaluate the overall performance of our Wi-PSG. Finally, we evaluate the performance of Wi-PSG under various factors and compare it with the state-of-the-art systems.

### A. Implementation

Wi-PSG uses a pair of wireless AP and WiFi device which is described in Section IV-B. More particularly, the laptop runs Ubuntu 12.04 LTS with the 3.2.14 kernel and is configured to work under *Client mode* with a packet transmission rate of 20 pkts/s at 2.4-GHz band unless mentioned otherwise. For each packet, Wi-PSG extracts CSI signals from 30 subcarriers at the RX. The ground truths of RMD movements are obtained by using a video camera (see Fig. 6). CSI data are processed and classified on the laptop using MATLAB R2018a.

*1) Experiment Environment:* We conduct experiments all experiments in a laboratory of 5.2 m × 6 m, where multiple chairs, desks, computers and wardrobes are placed, as illustrated in Fig. 17. The relative positions of the TX and RX are also shown in the figure. How the relative positions of transceiver affect the performance of Wi-PSG will be discussed in Section V-B. Furthermore, during our experiments, there may exist other students sitting or walking in the laboratory, which implies a complex and time-varying radio propagation environment. We will discuss various interference factors which could affect the performance of Wi-PSG in Section V-D.

*2) CSI Data Collection:* We conduct the experiments by recruiting nine volunteers, including six adults (three males and three females) and three children (two boys and one girl). Their ages are in the range of six to 27 years, with the weight from 20 to 65 kg. We ask each of the volunteers to take actions according to Table I for 240 times across one month. Note that each volunteer executes only one action at a time, we do take into account that multiple actions are performed simultaneously (e.g., rolling head while turning from supine to side). In total, we collect 8640 sequences of CSI signals. For each volunteer, we first randomly divide the CSI data into different subsets and then apply tenfold cross-validation to evaluate the performance of movement recognition.

*3) Evaluation Metrics:* We evaluate the accuracy of movement detection as follows:

$$\text{Detection accuracy} = \frac{R^D}{R^A} \times 100\% \tag{5}$$

where $R^D$ and $R^A$ represent the number of rhythmic movements detected by our Algorithms and the number of movements actually performed, respectively.

To evaluate the performance of movement recognition, we use the following three metrics as:

$$\text{Recognition accuracy} = \frac{\text{TP} + \text{TN}}{\text{TP} + \text{FP} + \text{TN} + \text{FN}} \times 100\% \tag{6}$$

where TP and FP represent true and false positive, TN and FN represent true and false negative, respectively

$$\text{F1} - \text{score} = \frac{2 \times \text{recall} \times \text{precision}}{\text{recall} + \text{precision}} \times 100\% \tag{7}$$

where recall $= [\text{TP}/(\text{TP} + \text{FN})]$, precision $= [\text{TP}/(\text{TP} + \text{FP})]$.

*Confusion Matrix:* The columns of the confusion matrix denote the ground truth, while the rows represent the classified (recognized) RMD movements. Each entry in the matrix represents the percentage of correctly classified RMD movements.

### B. Device Deployment

First, we investigate how the displacement of the AP and the WiFi device affects the measurements of CSI and therefore the recognition accuracy of Wi-PSG.

*1) Effect of Device Positions:* In this experiment, the AP and the WiFi device are placed at two sides of the bed with a distance of 2.5 m, and we study how the prorogation direction of wireless signals (i.e., the direction of the line connecting the AP and the WiFi device) affects the performance of Wi-PSG. To this end, we change the positions of the pair of AP and WiFi device from L1 (i.e., perpendicular to the bed) to L4 (i.e., parallel to the bed), illustrated in Fig. 17, and evaluate the performance of Wi-PSG under various positions. For each pair of positions, we randomly invite a volunteer to take actions according to Table I for 120 times, and run algorithms of Wi-PSG, and calculate the movement recognition accuracy according to (6). As shown in Fig. 18(a), the average recognition accuracy under four different device positions are 97.3%, 93.3%, 92.6%, and 70.2%, respectively. Particularly, Wi-PSG achieves best and worst performances on positions L1 and L4, especially the recognition accuracy of head rolling drops dramatically on L4. We speculate the reason is that, when wireless signals are transmitted perpendicular to the body, head movement is the most significant factor causing the changes of signal prorogation paths, which result in variations of CSI measurements. On the contrary, when wireless signals are transmitted parallel to the body, the main prorogation path of wireless signals is mostly blocked or interfered by the main part of the body no matter how the head moves, which implies the CSI measurements may not be changed obviously. Thus, in the following experiments, the two devices are placed on the direction perpendicular to the bed.

*2) Effect of Device Distances:* In this experiment, the AP and the WiFi devices are placed on the direction perpendicular to the bed with distances from 2 to 4 m at an interval of 0.5m. For each distance, we also randomly invite a volunteer to take actions according to Table I for 120 times, and run algorithms of Wi-PSG, and calculate the movement recognition accuracy

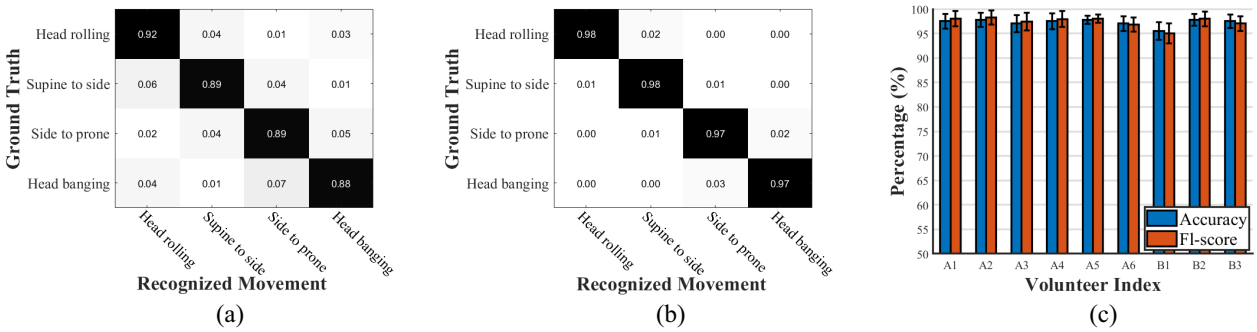


Fig. 20. Performance of movement recognition. (a) Without five extra features. (b) With five extra features. (c) Recognition accuracy/F1-score.

according to (6). As shown in Fig. 18(b), the average recognition accuracy under four different device distances are 97.3%, 97.1%, 94.5%, and 91.8%, respectively. Overall, we observe that the average recognition accuracy is higher than 90% which demonstrates that Wi-PSG is very accurate across different distances. In addition, shorter distance between the AP and the WiFi device results in better performance. For example, the average recognition accuracy is higher than 97% when the distance is under 3 m. We speculate that the reason is the received wireless signals are stronger with shorter communication distances, providing more reliable CSI measurements to capture the movements body parts. In the following experiments, we set the distance between the AP and the WiFi device as 3 m, considering that the typical width of a king-size bed is less than 2 m.

### C. Overall Performance

In this part, we evaluate the overall performance of Wi-PSG. The overall performance evaluation contains movement detection performance evaluation and movement recognition performance evaluation.

*1) Evaluation of Movement Detection:* In this experiment, we implement VitalSleep [20], and utilize its subcarrier selection scheme (based on the variance of CSI amplitudes) and peak selection (constant threshold-based) algorithm to conduct RMD movement detection, and compare its performance with our Wi-PSG. Fig. 19(a) compares the movement detection accuracies of Wi-PSG and VitalSleep for each individual volunteer. "A" and "Bj" represent adult $\sharp i$, and child $\sharp j$, respectively. It can be seen that the average movement detection accuracy of Wi-PSG exceeds 98% for all volunteers. This suggests that Wi-PSG can achieve highly accurate movement detection. By contrast, the detection accuracy of VitalSleep is below 85% for most volunteers. The main reason is that VitalSleep fails to find an optimal subcarrier and the constant threshold of peak detection cannot adapt to the change of the background model. As a result, comparing with Wi-PSG, VitalSleep suffers an average of 15.5% performance degradation.

Furthermore, Fig. 19(b) presents the detection accuracies of Wi-PSG for each kind of RMD movements separately. As we can see, the detection accuracies of body rolling (i.e., supine to side and side to prone) and head banging for all nine volunteers are 100% while the accuracy of head rolling decreases to 92% and 96% for B1 and B3. The reason is children tend to have small amplitudes of movements than adults, especially for those subtle movements like head rolling.

*2) Evaluation of Movement Recognition:* As a comparison, we first examine the movement recognition accuracies of each kind of movements, including head rolling, head banging, body rolling (i.e., supine to side and side to prone), without and with extra features. Fig. 20(a) reports the average recognition accuracies for all volunteers with only *six* primary features (i.e., SD, range, maximum, median, kurtosis, and skewness) in a confusion matrix and we observe the recognition accuracies for different movements are from 88% to 92%, and 7% head banging is incorrectly recognized as turning body from supine to side. By contrast, with *five* extra features (the subcarrier with maximum sensitivity, mean, minimum, variance, and sensitivity), the recognition accuracies are significantly improved. As shown in the confusion matrix in Fig. 20(b), the average recognition accuracies of all kinds of movements are above 97% and the error rate of misclassifying head banging to turning from supine to side is decreased to 3%. This comparison confirms the efficacy of the extra features.

In addition, Fig. 20(c) reports the movement recognition performance of Wi-PSG in terms of recognition accuracy and F1-score for each individual volunteer. It can be seen that, for most volunteers, both recognition accuracy and F1-score of Wi-PSG are above 97% and the SDs (black error bar) are under 1.5%. Although, for B1, Wi-PSG presents a slightly degraded performance, both its recognition accuracy and F1-score still exceed 95%. In conclusion, Wi-PSG achieves good movement recognition performance, even for children.

### D. Impact of Various Factors

In this section, we perform a detailed study of Wi-PSG performance under various factors, including obstacles, human activity interferences, packet transmission rates, movement frequency ranges and transceiver heights.

*1) Obstacles:* We evaluate Wi-PSG with obstacles of different materials, including a carton, a plank, and an iron box, which are commonly used materials in home environments, in between of AP and WiFi device such that the LOS path between them is completely blocked. The thickness of all obstacles is over 5 cm.

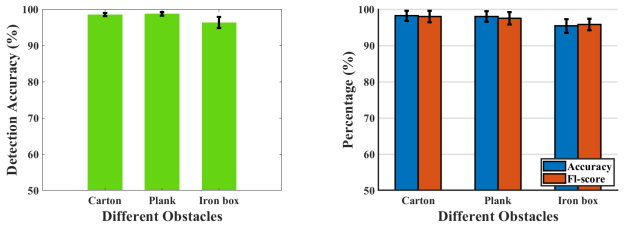


Fig. 21. Impact of obstacles. (a) Performance of movement detection. (b) Performance of movement recognition.

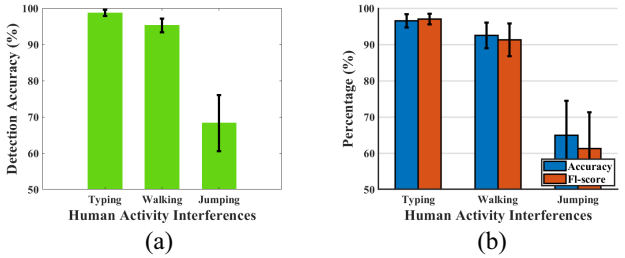


Fig. 22. Impact of human activity interferences. (a) Performance of movement detection. (b) Performance of movement recognition.

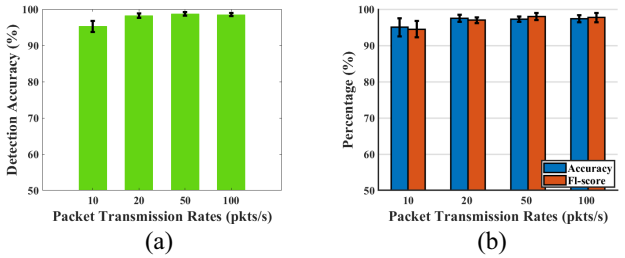


Fig. 23. Impact of packet transmission rates. (a) Performance of movement detection. (b) Performance of movement recognition.

From Fig. 21(a), we observe that average movement detection accuracy of Wi-PSG under different obstacles is above 96% and the SDs are under 1.6%. As illustrated in Fig. 21(b), the average recognition accuracy and F1-score of Wi-PSG under different obstacles are over 95% and 95%, respectively. Obviously, with the iron box, the performances of both movement detection and recognition are slightly worse than that of the carton and plank. It is reasonable since most of wireless signals will be reflected and absorbed by metal materials, which cause weaker CSI amplitude measurements. The results demonstrate that Wi-PSG works well under different obstacles.

*2) Human Activity Interferences:* In this experiment, when a volunteer is performing RMD related movements, another volunteer is asked to conduct unrelated activities simultaneously, including walking and jumping within a semicircular area with a radius of 1 m in front of the bed, and typing on the position marked as red star shown in Fig. 17.

From Fig. 22(a), we observe that, even under interferences of typing and walking, Wi-PSG maintains relatively high average movement detection accuracies, i.e., 98.7% and 95.3%,

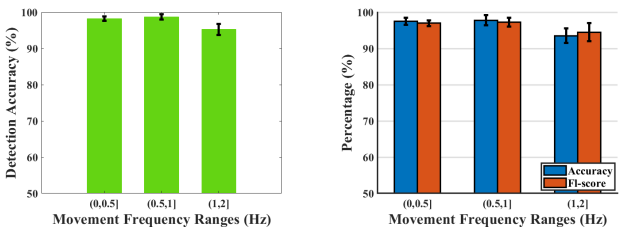


Fig. 24. Impact of movement frequency ranges. (a) Performance of movement detection. (b) Performance of movement recognition.

respectively. However, the detection accuracy drops dramatically to 68.3% under interference of jumping. Similarly, we can see from Fig. 22(b) that, under interferences of typing, the average recognition accuracy and F1-score of Wi-PSG are 96.5% and 97%, which is very close to that of no human activity interference, while both walking and jumping cause performance degradation of movement recognition. Particularly, the average recognition accuracy and F1-score decrease to 65% and 61.3% under interference of jumping. The results indicate that large amplitude motions like jumping can cause significant influence on the performance of Wi-PSG.

*3) Packet Transmission Rates:* As higher packet transmission rate provides more CSI amplitude measurements for detecting RMD movements, we further study how the packet transmission rate affects the performance of Wi-PSG. Fig. 23(a) and (b) present the performances of movement detection and recognition versus packet transmission rate when varying packet transmission rate from 10 to 100 pkts/s, respectively. We observe that, even with a packet transmission rate as low as 10 pkts/s, Wi-PSG achieves satisfactory movement detection and recognition accuracy, and F1-score, which are 95.2%, 95%, and 94.5%, respectively, and high packet transmission rate further improves the performance. Overall speaking, Wi-PSG is not very sensitive to packet transmission rate, especially when it is no less than 20 pkts/s. The results confirm that Wi-PSG can provide accurate RMD movement detection with a low packet transmission rate.

*4) Movement Frequency Ranges:* Since movement frequency of RMD ranges from 0.5 to 2 Hz, including slow movement (i.e., 0–0.5 Hz), normal movement (i.e., 0.5–1 Hz) and fast movement (i.e., 1–2 Hz), we further evaluate the performance of Wi-PSG under different movement frequency ranges.

Fig. 24(a) and (b) show the performances of movement detection and recognition of Wi-PSG under different movement frequency ranges. It can be seen that although the average accuracies of movement detection and recognition decrease a bit as the movement frequency ranges increase, Wi-PSG still achieve satisfactory movement detection and recognition accuracy, and F1-score, which are above 95%, 93%, and 94%, respectively. The results confirm that Wi-PSG can detect and recognize RMD related movements accurately (i.e., above 93%) no matter the movement frequency of RMD is slow, normal or fast.

*5) Transceiver Heights:* In this experiment, we study the performance of Wi-PSG by placing the wireless TX and RX

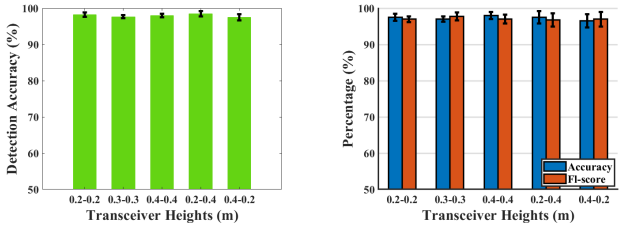


(a) (b)

Fig. 25. Impact of transceiver heights. (a) Performance of movement detection. (b) Performance of movement recognition.

at different heights. Specifically, we first examine three cases where the transceivers are placed at equal heights, i.e., 0.2, 0.3, and 0.4 m. Note that the height mentioned here refer to a relative height between transceivers and the upper surface of the bed. Then, we further study some real-world scenarios, where the heights of TX and RX are unequal, i.e., 0.2–0.4 m and 0.4–0.2 m.

Fig. 25(a) shows the average movement detection accuracy of Wi-PSG under five different transceiver heights. We observe that Wi-PSG achieve comparable high performances with various transceiver height placements. In general, the average movement detection accuracy of Wi-PSG under different transceiver heights is above 97% and the SDs are under 1%. As illustrated in Fig. 25(b), the average movement recognition accuracy and F1-score of Wi-PSG under different transceiver heights are above 96.5% and 96.8%, respectively. The results confirm that our Wi-PSG is robust to different transceiver heights on RMD movement detection.

### *E. In Comparison to the State-of-the-Art Systems*

In this part, we compare Wi-PSG with the state-of-the-art sleep monitoring systems. Since most existing technologies do not support both movement detection and recognition, we compare the performances of movement detection and recognition, separately.

For the sleep related movement detection, we compare our Wi-PSG with Wi-Sleep [19], Sleepy [47], and SleepGuard [9], and summarize the movement detection accuracies reported in each system as shown in Table III. It can be seen that Wi-PSG outperforms WiFi-based systems (i.e., Wi-Sleep and Sleepy) with 9.27% and 2.96% improvement of the detection accuracy. Compared with wearable device-based system (i.e., SleepGuard), Wi-PSG gains 6% improvement of the detection accuracy.

For the sleep related movement recognition, we compare Wi-PSG against SleepGuard [9], TagSheet [25], and TagSleep [17], and summarize the movement recognition accuracies reported in Table IV. Both TagSheet and TagSleep are RFID-based systems, which require a dedicated Impinj Speedway R420 reader, a directional antenna and a number of tags. As we can see, all comparison methods only recognize whole-body movements, i.e., distinguishing between turning from supine to side and turning from side to prone. For the whole-body movements, compared with the comparison methods, Wi-PSG can achieve comparable performance without wearing or deploying any dedicated device. Besides, Wi-PSG is able to recognize other two typical head movements, i.e., heading rolling and banging, with an accuracy of 98% and 97%, respectively.

TABLE III
COMPARISON OF DETECTION ACCURACY

| **Method** | Wi-Sleep | Sleepy | SleepGuard | **Wi-PSG** |
|---|---|---|---|---|
| **Accuracy** | 88.73% | 95.04% | 92% | 98% |

TABLE IV
COMPARISON OF RECOGNITION ACCURACY

| **Method** | **Head rolling** | **To side** | **To prone** | **Head banging** |
|---|---|---|---|---|
| SleepGuard | - | 98% | 96.4% | - |
| TagSheet | - | 100% | 91% | - |
| TagSleep | - | 98.39% | 99.67% | - |
| **Wi – PSG** | **98%** | **98%** | **97%** | **97%** |

## VI. DISCUSSION

Wi-PSG takes the first step of RMD movement detection and recognition by exploiting existing COTS WiFi. Limitations and opportunities for further improvement are discussed as follows.

### *A. Identifying Other Micromovements*

Wi-PSG has the potential for recognizing other micromovements (e.g., tonic-clonic seizure and bruxism) by utilizing high gain directional antennas to improve the power of transmitted and received signals, such that the minute changes of received CSI signals caused by micromovements can be captured.

### *B. Cross-Domain Recognition*

In common with existing works, the performance of Wi-PSG is domain (e.g., location, orientation, user, environment) dependent. Model trained using data collected with a particular user in a particular environment cannot be applied to other users or different environments directly. How to apply advanced machine learning technologies (like transfer learning) to enable cross-domain recognition is left for future work.

### *C. Multiuser Scenario*

Wi-PSG does not consider the scenario in which two or more people sleep on the same bed. The changes of received CSI signals caused by movements of different people will be superimposed together. It is challenging to decouple the superimposition of CSI measurements such that the movements of each person can be recognized, separately. We leave this as our future work.

## VII. Conclusion

In this article, we introduce a contactless and nonintrusive sleep monitoring system, named Wi-PSG by using COTS WiFi. Wi-PSG leverages the changes of CSI information caused by human movements to recognize typical subtypes of RMD movements accurately without requiring dedicate hardware. Comprehensive real-world experiments over a one-month time period confirm that the average detection and recognition accuracies of Wi-PSG are higher than 98% and 97%, respectively, which are comparable or even better as compared to existing dedicated sensor-based or RF-based approaches. Wi-PSG can be integrated in the existing WiFi infrastructures seamlessly, and thus constitutes a practical solution in practice.

## References


[1] *International Classification of Sleep Disorders—3rd Edition*, Amer. Acad. Sleep Med., Darien, IL, USA, 2014.

[2] M. Thorpy, *Classification of Sleep Disorders*. Cham, Switzerland: Springer Int., 2015.

[3] A. S. Walters *et al.*, "Review of the possible relationship and hypothetical links between attention deficit hyperactivity disorder (ADHD) and the simple sleep related movement disorders, parasomnias, hypersomnias, and circadian rhythm disorders," *J. Clin. Sleep Med.*, vol. 4, no. 6, p. 591, 2008.

[4] P. Gharagozlou, M. Seyffert, R. Santos, and S. Chokroverty, "Rhythmic movement disorder associated with respiratory arousals and improved by CPAP titration in a patient with restless legs syndrome and sleep apnea," *Sleep Med.*, vol. 10, no. 4, pp. 501–503, 2009.

[5] K. S. Carlock, J. P. Williams, and G. C. Graves, "MRI findings in headbangers," *Clin. Imag.*, vol. 21, no. 6, pp. 411–413, 1997.

[6] C. A. Kushida *et al.*, "Practice parameters for the indications for polysomnography and related procedures: An update for 2005," *Sleep*, vol. 28, no. 4, pp. 499–523, 2005.

[7] X. Guo, J. Liu, and Y. Chen, "FitCoach: Virtual fitness coach empowered by wearable mobile devices," in *Proc. INFOCOM*, 2017, pp. 1–9.

[8] X. Sun, L. Qiu, Y. Wu, Y. Tang, and G. Cao, "SleepMonitor: Monitoring respiratory rate and body position during sleep using smartwatch," *Proc. ACM Interact. Mobile Wearable Ubiquitous Technol.*, vol. 1, no. 3, pp. 1–22, 2017.

[9] L. Chang *et al.*, "SleepGuard: Capturing rich sleep information using smartwatch sensing data," *Proc. ACM Interact. Mobile Wearable Ubiquitous Technol.*, vol. 2, no. 3, pp. 1–34, 2018.

[10] S. Sadanand and J. J. Corso, "Action bank: A high-level representation of activity in video," in *Proc. CVPR*, 2012, pp. 1234–1241.

[11] M. Bartula, T. Tigges, and J. Muehlsteff, "Camera-based system for contactless monitoring of respiration," in *Proc. 35th Annu. Int. Conf. IEEE Eng. Med. Biol. Soc. (EMBC)*, 2013, pp. 2672–2675.

[12] L. A. M. Aarts *et al.*, "Non-contact heart rate monitoring utilizing camera photoplethysmography in the neonatal intensive care unit—A pilot study," *Early Human Develop.*, vol. 89, no. 12, pp. 943–948, 2013.

[13] M. Patino *et al.*, "Accuracy of acoustic respiration rate monitoring in pediatric patients," *Pediatric Anesthesia*, vol. 23, no. 12, pp. 1166–1173, 2013.

[14] T. Wang *et al.*, "Contactless respiration monitoring using ultrasound signal with off-the-shelf audio devices," *IEEE Internet Things J.*, vol. 6, no. 2, pp. 2959–2973, Oct. 2018.

[15] K. Qian *et al.*, "Acousticcardiogram: Monitoring heartbeats using acoustic signals on smart devices," in *Proc. INFOCOM*, 2018, pp. 1574–1582.

[16] R. Ravichandran *et al.*, "WiBreathe: Estimating respiration rate using wireless signals in natural settings in the home," in *Proc. IEEE Int. Conf. Pervasive Comput. Commun. (PerCom)*, 2015, pp. 131–139.

[17] C. Liu *et al.*, "Beyond respiration: Contactless sleep sound-activity recognition using RF signals," *ACM Interact. Mobile Wearable Ubiquitous Technol.*, vol. 3, no. 3, pp. 1–22, 2019.

[18] F. Adib, H. Mao, Z. Kabelac, D. Katabi, and R. C. Miller, "Smart homes that monitor breathing and heart rate," in *Proc. 33rd Annu. ACM Conf. Human Factors Comput. Syst.*, 2015, pp. 837–846.

[19] X. Liu, J. Cao, S. Tang, and J. Wen, "Wi-Sleep: Contactless sleep monitoring via WiFi signals," in *Proc. IEEE Real-Time Syst. Symp. (RTSS)*, 2014, pp. 346–355.

[20] J. Liu *et al.*, "Tracking vital signs during sleep leveraging off-the-shelf WiFi," in *Proc. 16th ACM Int. Symp. Mobile Ad Hoc Netw. Comput. (ACM MobiHoc)*, 2015, pp. 267–276.

[21] J. Liu, Y. Chen, Y. Wang, X. Chen, J. Cheng, and J. Yang, "Monitoring vital signs and postures during sleep using WiFi signals," *IEEE Internet Things J.*, vol. 5, no. 3, pp. 2071–2084, Jun. 2018.

[22] N. Pombo and N. M. Garcia, "ubiSleep: An ubiquitous sensor system for sleep monitoring," in *Proc. IEEE 12th Int. Conf. Wireless Mobile Comput. Netw. Commun. (WiMob)*, 2016, pp. 1–4.

[23] J.-K. Min, A. Doryab, J. Wiese, S. Amini, J. Zimmerman, and J. I. Hong, "Toss'n'turn: Smartphone as sleep and sleep quality detector," in *Proc. SIGCHI Conf. Human Factors Comput. Syst.*, 2014, pp. 477–486.

[24] W. Gu, L. Shangguan, Z. Yang, and Y. Liu, "Sleep hunter: Towards fine grained sleep stage tracking with smartphones," *IEEE Trans. Mobile Comput.*, vol. 15, no. 6, pp. 1514–1527, Jul. 2015.

[25] J. Liu, X. Chen, S. Chen, X. Liu, Y. Wang, and L. Chen, "TagSheet: Sleeping posture recognition with an unobtrusive passive tag matrix," in *Proc. INFOCOM*, 2019, pp. 874–882.

[26] J. Paquet, A. Kawinska, and J. Carrier, "Wake detection capacity of actigraphy during sleep," *Sleep*, vol. 30, no. 10, pp. 1362–1369, 2007.

[27] A. Kosmadopoulos, C. Sargent, D. Darwent, X. Zhou, and G. D. Roach, "Alternatives to polysomnography (PSG): A validation of wrist actigraphy and a partial-PSG system," *Behav. Res. Methods*, vol. 46, no. 4, pp. 1032–1041, 2014.

[28] H. Zhu, J. Hu, S. Chang, and L. Lu, "ShakeIn: Secure user authentication of smartphones with habitual single-handed shakes," *IEEE Trans. Mobile Comput.*, vol. 16, no. 10, pp. 2901–2912, Sep. 2017.

[29] B. Fang, N. D. Lane, M. Zhang, A. Boran, and F. Kawsar, "BodyScan: Enabling radio-based sensing on wearable devices for contactless activity and vital sign monitoring," in *Proc. 14th Annu. Int. Conf. Mobile Syst. Appl. Services (ACM MobiSys)*, 2016, pp. 97–110.

[30] B. Fang, N. D. Lane, M. Zhang, and F. Kawsar, "HeadScan: A wearable system for radio-based sensing of head and mouth-related activities," in *Proc. 15th ACM/IEEE Int. Conf. Inf. Process. Sensor Netw. (IPSN)*, 2016, pp. 1–12.

[31] Y. Chen, L. Yu, K. Ota, and M. Dong, "Robust activity recognition for aging society," *IEEE J. Biomed. Health Informat.*, vol. 22, no. 6, pp. 1754–1764, Mar. 2018.

[32] Y. Chen, L. Yu, K. Ota, and M. Dong, "Hierarchical posture representation for robust action recognition," *IEEE Trans. Comput. Soc. Syst.*, vol. 6, no. 5, pp. 1115–1125, Sep. 2019.

[33] A. D. Droitcour, O. Boric-Lubecke, and G. T. A. Kovacs, "Signal-to-noise ratio in Doppler radar system for heart and respiratory rate measurements," *IEEE Trans. Microw. Theory Techn.*, vol. 57, no. 10, pp. 2498–2507, Oct. 2009.

[34] P. Nguyen, X. Zhang, A. Halbower, and T. Vu, "Continuous and fine-grained breathing volume monitoring from afar using wireless signals," in *Proc. INFOCOM*, 2016, pp. 1–9.

[35] J. Salmi and A. F. Molisch, "Propagation parameter estimation, modeling and measurements for ultrawideband MIMO radar," *IEEE Trans. Antennas Propag.*, vol. 59, no. 11, pp. 4257–4267, Aug. 2011.

[36] F. Adib, Z. Kabelac, D. Katabi, and R. C. Miller, "3D tracking via body radio reflections," in *Proc. 11th USENIX Symp. Netw. Syst. Design Implement. (NSDI)*, 2014, pp. 317–329.

[37] M. Zhao, F. Adib, and D. Katabi, "Emotion recognition using wireless signals," in *Proc. 22nd Annu. Int. Conf. Mobile Comput. Netw.*, 2016, pp. 95–108.

[38] M. Zhao *et al.*, "Through-wall human pose estimation using radio signals," in *Proc. IEEE Conf. Comput. Vis. Pattern Recognit. (CVPR)*, 2018, pp. 7356–7365.

[39] S. Sigg, M. Scholz, S. Shi, Y. Ji, and M. Beigl, "RF-sensing of activities from non-cooperative subjects in device-free recognition systems using ambient and local signals," *IEEE Trans. Mobile Comput.*, vol. 13, no. 4, pp. 907–920, Feb. 2013.

[40] M. B. Khan *et al.*, "Design of software defined radios based platform for activity recognition," *IEEE Access*, vol. 7, pp. 31083–31088, 2019.

[41] W. Xi *et al.*, "Device-free human activity recognition using CSI," in *Proc. 1st Workshop Context Sens. Activity Recognit.*, 2015, pp. 31–36.

[42] M. Hussain, L. Lu, and H. Zhu, "A cross-layer RF distance bounding realization for passive wireless devices," *IEEE Trans. Wireless Commun.*, vol. 14, no. 6, pp. 3076–3085, Feb. 2015.

[43] X. Liu, J. Cao, S. Tang, J. Wen, and P. Guo, "Contactless respiration monitoring via off-the-shelf WiFi devices," *IEEE Trans. Mobile Comput.*, vol. 15, no. 10, pp. 2466–2479, Oct. 2015.

[44] X. Wang, C. Yang, and S. Mao, "PhaseBeat: Exploiting CSI phase data for vital sign monitoring with commodity WiFi devices," in *Proc. IEEE 37th Int. Conf. Distrib. Comput. Syst. (ICDCS)*, 2017, pp. 1230–1239.
[45] Y. Zhuo, H. Zhu, and H. Xue, "Identifying a new non-linear CSI phase measurement error with commodity WiFi devices," in *Proc. IEEE ICPADS*, 2016, pp. 72–79.
[46] H. Zhu, Y. Zhuo, Q. Liu, and S. Chang, "Pi-splicer: Perceiving accurate CSI phases with commodity WiFi devices," *IEEE Trans. Wireless Commun.*, vol. 17, no. 9, pp. 2155–2165, Jan. 2018.
[47] Y. Gu, J. Zhan, Z. Liu, J. Li, Y. Ji, and X. Wang, "Sleepy: Adaptive sleep monitoring from afar with commodity WiFi infrastructures," in *Proc. IEEE Wireless Commun. Netw. Conf. (WCNC)*, 2018, pp. 1–5.
[48] H. Li, K. Ota, M. Dong, and M. Guo, "Learning human activities through Wi-Fi channel state information with multiple access points," *IEEE Commun. Mag.*, vol. 56, no. 5, pp. 124–129, May 2018.
[49] D. Halperin, W. Hu, A. Sheth, and D. Wetherall, "Predictable 802.11 packet delivery from wireless channel measurements," *ACM SIGCOMM Comput. Commun. Rev.*, vol. 40, no. 4, pp. 159–170, 2010.
[50] J. D. Villasenor, B. Belzer, and J. Liao, "Wavelet filter evaluation for image compression," *IEEE Trans. Image Process.*, vol. 4, no. 8, pp. 1053–1060, Aug. 1995.
[51] X. Xu *et al.* "BreathListener: Fine-grained breathing monitoring in driving environments utilizing acoustic signals," in *Proc. 17th Annu. Int. Conf. Mobile Syst. Appl. Services (ACM MobiSys)*, 2019, pp. 54–66.
[52] Y. Sun, C. Wang, and W. Yin, "Sleep related rhythmic movement disorder," *Chin. J. Neuroimmunol. Neurol.*, vol. 25, no. 5, pp. 359–362, 2018.

**Wei Liu** received the M.S. degree from the School of Information and Communication Engineering, Hainan University, Haikou, China, in 2018. He is currently pursuing the Ph.D. degree with the School of Computer Science and Technology, Donghua University, Shanghai, China.

His research interests include ubiquitous and pervasive computing, mobile computing/sensing, and edge computing.

**Shan Chang** (Member, IEEE) received the Ph.D. degree in computer software and theory from Xi'an Jiaotong University, Xi'an, China, in 2013.

From 2009 to 2010, she was a Visiting Scholar with the Department of Computer Science and Engineering, Hong Kong University of Science and Technology, Hong Kong. She was also a Visiting Scholar with BBCR Research Lab, University of Waterloo, Waterloo, ON, Canada, from 2010 to 2011. She is currently an Associate Professor with the Department of Computer Science and Technology, Donghua University, Shanghai, China. Her research interests include security and privacy in mobile networks and sensor networks.

Dr. Chang is a member of IEEE Computer Society, Communication Society, and Vehicular Technology Society.

**Ye Liu** received the M.S. degree from the Department of Software Engineering, Kunming University of Science and Technology, Kunming, China, in 2019. She is currently pursuing the Ph.D. degree with the School of Computer Science and Technology, Donghua University, Shanghai, China.

Her research interests include ubiquitous and pervasive computing, privacy, and security of federated learning.

**Hao Zhang** received the bachelor's degree from Shanghai Ocean University, Shanghai, China, in 2019. He is currently pursuing the postgraduation degree with the School of Computer Science and Technology, Donghua University, Shanghai, China.

His research interests include Internet of Things, privacy protection, and federated learning.